

Novel Approach for Suppressing of Hot Cracking Via Magneto-fluid Dynamic Modification of the Laser-Induced Marangoni Convection

A. Seidel, L. Degener, J. Schneider, F. Brueckner, E. Beyer, and C. Leyens

Abstract

The occurrence of hot cracking is a significant problem during welding processing of highly heat resistant nickel-base superalloys. Hot cracking is most often associated with liquid films that are present along grain boundaries in the fusion zone and the partially melted zone and can only be suppressed to a very limited extent. The latter is the case despite remarkable studies and analyses of the phenomenon. In this work, a new approach is presented which intends the suppression of hot cracking by using a non-contact method to influence the solidification process. It is based on the idea of a modification of the laser-induced melt pool convection (Marangoni convection) using customized magnetic fields. As a consequence, special system technology is derived on the basis of theoretical considerations while the effectiveness to be expected is estimated on the basis of the information available in the literature. The implemented system technology is described in detail. The focus of this description is on the magnetic flux density distribution or the temporal change, respectively, with respect to the laser-induced melt pool. The presented experimental results provide a comparative view of samples welded with and without the influence of a magnetic field while a significant difference is evident. The outlook of this work describes key data of a test stand specially developed for examining the identified topic in in-depth investigations.

Keywords

Laser metal deposition • Magneto-fluid dynamics • Hybrid manufacturing • Hot cracking • Nickel-base superalloys • Mar-M-247

Derivation of a Novel Approach

Introduction and Motivation

Laser Metal Deposition (LMD) is classified as a direct energy deposition process in which highly concentrated energy is used to bond the filler material and the substrate material by using strongly localized heat input, resulting in a distinctive narrow heat-affected zone (HAZ) Within LMD high-temperature materials are an important area of research because of their excellent resistance to mechanical and chemical degradation under thermal exposure [2]. One example is the Ni-based superalloy Mar-M-247. The alloy was developed in the early nineteen-seventies by the Martin Marietta Corporation and contains eleven elements beside the base element nickel [3]. Gunderson et al. [4] evaluate Mar-M-247 as one of the most difficult alloys to be processed by conventional fusion welding due to its distinct tendency for hot cracking. These cracks are linked to the interval between the liquidus and solidus temperatures and occur intercrystalline and/or interdendritic. After their local occurrence, a distinction is made between solidification cracking and heat-affected zone liquation cracking. There are a variety of strategies to avoid hot cracking such as metallurgical measures like the adjustment of the base material [5], the filler material [6], the process gas [7], the adjustment of the melt pool dimensions [8], the superimposition of

Fraunhofer Institute for Machine Tools and Forming Technology, Nöthnitzer Straße 44, 01187 Dresden, Germany e-mail: Andre Seidel@iwu.fraunhofer.de

L. Degener · J. Schneider · F. Brueckner · E. Beyer · C. Leyens Fraunhofer Institute for Material and Beam Technology, Winterbergstraße 28, Dresden, Germany

A. Seidel · L. Degener · J. Schneider · E. Beyer · C. Leyens Technische Universität Dresden, Helmholtzstraße 7, 01069 Dresden, Germany

F. Brueckner Luleå University of Technology, 971 87 Luleå, Sweden

A. Seidel (⊠)

compressive stresses [9], adjusted temperature control [10], or a combination of these in terms of thermomechanical control [11–13], as well as magneto-fluid dynamic measures [14], which are addressed herein.

Laser-Induced Melt Pool, Solidification and the Phenomenon of Hot Cracking

The applied laser beam has a Gaussian intensity distribution whereby the induced melt pools show a maximum temperature in the center decreasing toward solidification temperature at the phase boundaries (Fig. 1). As a consequence, there is a temperature-induced gradient of the surface tension at the liquid-gas interface [15–18]. The latter is the predominant driving force of the Marangoni convection. According to Wu [17], the flow velocity value lies within the magnitude of 10–100 cm/s, while Brückner [13] notes that the interaction is limited to the region in the proximity of the liquid-gas interface.

Concept of Magneto-Fluid Dynamic Modification of the Laser-Induced Marangoni Convection

The Mushy Zone is regarded as an area in which the melt flows through the solidifying dendritic network, which is understood as a porous matrix in which a lack of melt supply can lead to pores or hot tears [19, 20]. Moreover, gaseous inclusions such as air, hydrogen, nitrogen and/or carbon monoxide frequently act as a preferred starting point for cracks [19]. The cracks, on the other hand, occur due to the decrease in volume from the phase change from liquid to solid, i.e., cooling-related shrinkage in combination with effective tensile stresses. The cracking, however, starts, if the partial pressure drop cannot be compensated by adequate melt supply [12]. In previous works, it was assumed that a strong melt flow could enable mechanically shearing off the

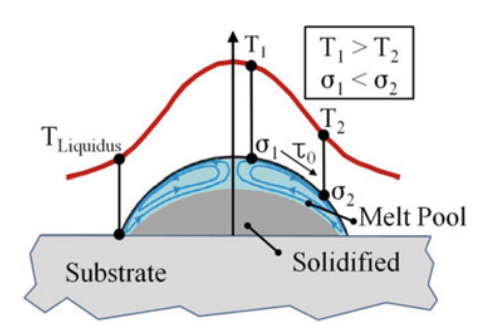


Fig. 1 Temperature-induced gradient of the surface tension and the resulting Marangoni convection with qualitative presentation of the temperature T, the surface tension σ and the shear stress τ reprinted with permission from ref (Reproduced from [1])

dendrites near the solidification front [21-26] which, however, could improve the supply of melt. Nevertheless, this assumption was disproved experimentally by Moeinipour et al. [27]. The authors showed that the forces determined from the magnetically induced turbulent flow were orders of magnitudes lower than those required for shearing off. A theoretical work by Ananiev et al. [28] supports the findings that shearing off the dendrites due to purely mechanical stress cannot to be expected, but attests to a substantial role in fragmentation. According to the current state of research, it is assumed that the fragmentation of dendrites can be achieved by an appropriate combination of mechanically induced curvature undercooling and solute undercooling at the solid-liquid phase boundary, while experimental evidence for this hypothesis is provided by Liotti et al. [29]. In fact, by in situ observation Liotti et al. demonstrated that solute-rich interdendritic liquid, circulated by pulsed electromagnetic fields (PEMF), can cause the dendrites to melt (Fig. 2).

Liotti et al. refer to this as an intrinsic method of grain refining, since the effectiveness is distributed across all areas of the mushy zone not being linked to the proportion of liquid phases. As a consequence, Liotta et al. conclude that fragmentation is caused by the induced interdendritic flows, which could further be used to control the microstructure.

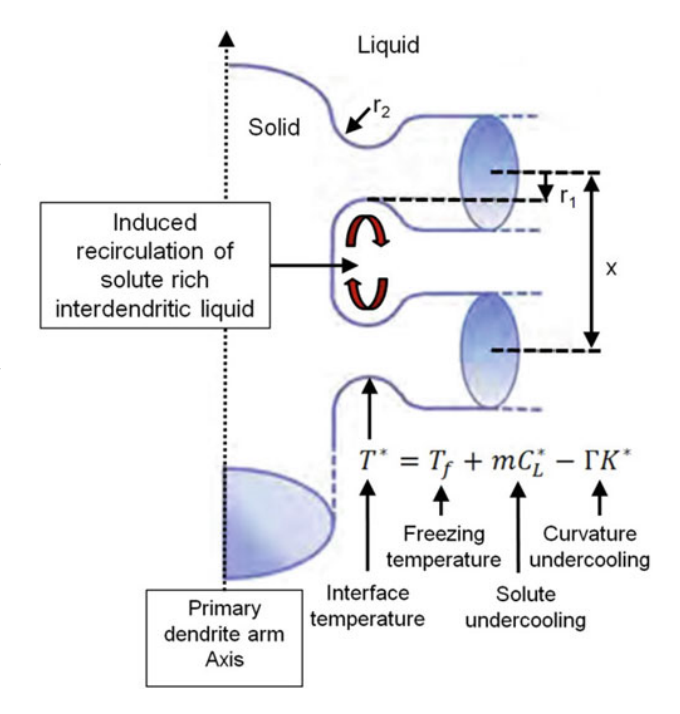


Fig. 2 Schematic representation of the secondary arms of a dendrite. Therein, the secondary arm distance X, the curvature of the root of the secondary arms is described by the radii r_1 and r_2 , the temperature at the phase boundary, which is composed of the parts solidification temperature, constitutional undercooling and curvature undercooling. And representation of the pulsed electromagnetic-field-induced interdendritic circulation (Reproduced from Liotti et al. 2016)

On this basis, it is concluded that a similar effect may be achieved by influencing the laser-induced movement of the melt pool (Marangoni flow) using magnetic fields.

Magnetic Flow Control and Energy Dissipation

Magnetic fluid dynamics (MFD) are characterized by flow phenomena that do not occur in conventional hydrodynamics. An example of such a flow structure is the Hartmann flow [30, 31]. The latter arises in the flow of an electrically conductive liquid, if penetrated by a constant magnetic field orientated perpendicular to the flow direction as shown and described for an electrically nonconductive rectangular channel [30, 32]. The interaction of such an external magnetic field \vec{B} with the traversing electrical conductor, moving with the velocity field \vec{U} , generates a potential difference and thus an electrical current \vec{I} , while the interaction of both generates a Lorentz force \vec{F}_L . Due to conservation of charge (div $\vec{I} = 0$), the potential difference generated by $\vec{U} \times \vec{B}$ results in closed electrical current lines [33] (Fig. 3a), which again results in a position-dependent orientation of the Lorentz force (Fig. 3b) determined by the sign of the current direction ($\vec{F}_L = \pm \vec{I} \times \vec{B}$). As a result, the parabolic velocity profile of the Hagen-Poiseuille flow $\vec{U}_{X,HP}(y)$ is converted into the profile of the Hartmann flow $\vec{U}_{XHS}(y)$ due to the velocity reducing or accelerating effect of the Lorentz force [34] (Fig. 3a, b). The Hartmann number Ha, however, is frequently used to assess the influence on the flow profile to be expected (c.f. Fig. 3c) [30, 32, 33, 35–38]. Either way, a significant increase of the velocity gradient in proximity to the channel wall causes an increase of frictional forces, which leads to an increased intensity of heat transfer at the phase boundary [39].

Hypothesis of a Novel Approach

A significant growth in the velocity gradient at the channel wall causes rising frictional forces, resulting in an increased intensity of heat transfer at the interface. A significant increase in flow velocity, on the other hand, enables effective dissipation of the kinetic energy. Either way, Liotti et al. demonstrated that the interface temperature can be elevated through appropriate pairing of solute undercooling and curvature undercooling, which was achieved magneto-fluid dynamic flow control, resulting in the fragmentation of primary and secondary dendrites. The latter, however, even in areas with a small amount of liquid phase. As a consequence, the hypothesis is drawn that such an effect may be achieved by the modification of the laser-induced Marangoni convection with an external magnetic field. This is done, however, to potentially improve the supply of melt in order to compensate for the mechanisms that lead to hot cracking. This shall be achieved by synergetic combination of adequate gradients of the surface tension (beam profile and intensity distribution), appropriate duration of laser-material interaction (feed rate and/or exposure time) as well as the magnitude and orientation of the applied magnetic field.

Attempt to Evaluate Effectiveness

An important criterion that is used to evaluate the occurrence of magneto-fluid-dynamic-induced boundary layer phenomena is the Hartmann number Ha (Eq. 1) [30, 32, 40, 41]. It is a dimensionless ratio of the viscous and the electromagnetically induced friction forces [42–44]. Either way, the strength of the applied magnetic flux density B, a characteristic length L, the electrical conductivity σ and the

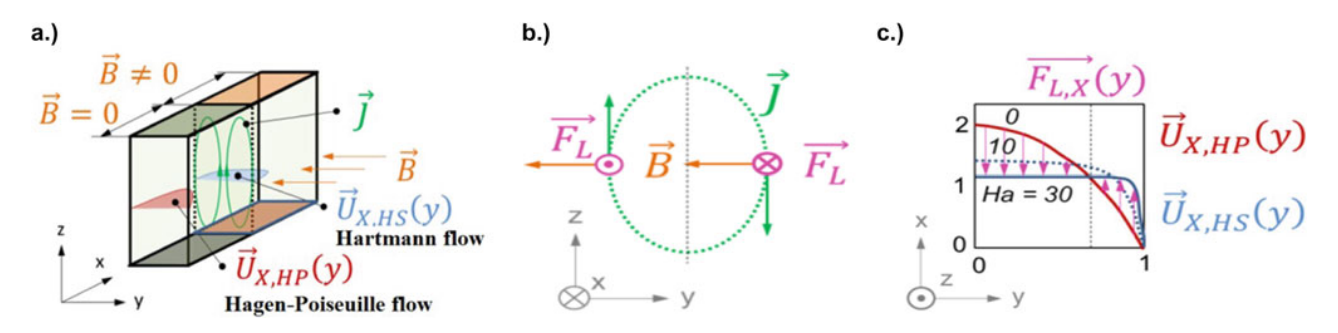


Fig. 3 a Representation of a Hagen-Poiseuille flow flowing along the channel wall (phase boundary) in the X direction, which changes into a Hartmann flow under the influence of a non-zero and temporally constant magnetic flux density \vec{B} acting in the minus Y direction creating a potential difference \vec{I} while forming closed electric current

lines; \mathbf{b} orientation of the Lorentz force depending on the direction of the electrical current; \mathbf{c} transformation of the Hagen-Poiseuille flow into the Hartmann flow through that of the location-dependent orientation of the Lorentz force

dynamic viscosity η are used for calculation. The characteristic length represents the width of the melt penetrated by the magnetic field (c.f. channel thickness in the Y direction shown in Fig. 3a) the dynamic viscosity and the electrical conductivity are temperature-dependent variables, for the resistance that the melt opposes to its own flow. However, the influence of the magnitude of the Hartmann number on the flow profile is shown in Fig. 3c for Ha = 0, 10 and 30.

$$Ha = B \cdot L \cdot \sqrt{\frac{\sigma}{\eta}} \tag{1}$$

The values for the magnetic field and the characteristic length are determined by the experimental setup while the value for the root term should obviously be as high as possible (Eq. 1). For Mar-M-247, the material parameters, could not be found in the literature. Therefore, this section makes an estimate based on related alloy (Table 1) and expedient assumptions (Table 2).

The electrical conductivity has not yet been determined for the high-temperature alloys mentioned in Table 1, or at least not in the relevant temperature range above the liquidus temperature. The extrapolation of the conductivity from the solid is only possible to a limited extent, due to the presence of the intermetallic γ' phase representing another material from a thermophysical point of view, as experimentally determined by Roebuck et al. [46]. In fact, the specific electrical resistance, the inverse of the electrical conductivity, was determined by Roebuck et al. in the temperature interval from RT to approx. 1250 °C for CMSX-4. Thus, staying below the solidus temperature (see Table 1) and below the solution temperature of the γ' precipitations, which is expected in the range of 1329 °C [47]. The results show that the specific electrical resistance decreases sharply above approximately 800 °C up to the maximum measuring temperature. Roebuck et al. [46] attribute this to the beginning dissolution of the γ' precipitations. Accordingly, it may be assumed that the decrease of specific electrical resistance continues until the γ' precipitations have dissolved. The dynamic viscosity for CM247-LC and CMSX-4 was determined experimentally by Sato et al. [52] in the temperature interval from 1358 to 1603 °C. Based on the findings of Roebuck et al. and Sato et al., the subsequent values are used to evaluate the effectiveness (Table 2).

Using the values from Table 2 and Eq. 1, a noticeable influence on the flow is expected for a melt pool width in the range of 2 mm in combination with a magnetic flux density in the magnitude of 300 mT. Noticeable, however, is associated here with Ha = 10 in reference to Fig. 3c.

Experimental Procedure to Investigate the Hypothesis of the Novel Approach

Hybrid System Technology

A drop-shaped electromagnet with a maximum internal diameter of 125 mm is made of a round steel core (S235 JR) with an overall length of 500 mm and a cross-sectional diameter of 10 mm (Fig. 4a). The pole legs of the electromagnet leave the base circle tangentially running at an angle of 45° toward the X-Y working plane (Fig. 4a, b). The minimum distance between the pole shoes of the electromagnet is 10,125 mm in the X direction as indicated in Fig. 4c (detail). Furthermore, the steel core is surrounded by 80 single-core copper wire windings (40 per pole leg) with a 3 mm conductor cross section insulated by 0.5 mm thick polyvinyl chloride. The steel core is fixed in an aluminum clamp bracket (Fig. 4b). The holding device for the electromagnet is equipped with 3 single-axis positioning tables (reading accuracy 0.01 mm) as adjustment units for the spatial directions X, Y and Z (Fig. 4b). The holding device is mounted to the Z-axis of a 5-axis CNC machining center of type Hermle C 800 U which is further equipped with a coaxial process head of type Fraunhofer IWS COAXpowerline for laser metal deposition with powder. The electromagnet is operated with a power source of type Xantrex XFR 20-60 supplying an output current of up to 60 A. The magnetic field is measured with a temperaturecompensated Magnetometer of type KOSHAVA 5 from the company Wuntronic. The Magnetometer is equipped with a transversal probe of type OW2-TT-3R with an active measuring area in a 5-by-5-mm square as indicated by the red measuring tip in Fig. 4c. Figure 4d, however, shows the experimental setup illustrating the penetration of the laser-induced melt pool by the magnetic field.

Table 1 Nominal chemical composition of the superalloys Mar-M-247, CM247-LC and CMSX-4 in M% according to [45] and Melting temperature intervals of the alloys Mar-M-247 [45, 48], CM247-LC [49, 50] and CMSX-4 [51]

	Ni (M%)	Co (M%)	W (M%)	Cr (M%)	Al (M%)	Ta (M%)	Hf (M%)	Ti (M%)	Mo (M%)	C (M%)	Zr (M%)	B (M%)	T _{Solidus} (°C)	T_{Liquidus} (°C)
Mar-M-247	59.69	10	10	8.4	5.5	3	1.5	1	0.7	0.15	0.05	0.015	1245	1313
CM247-LC	61.87	9.2	9.5	8	5.6	3.2	1.4	0.7	0.5	0	0.015	0.015	1250	1298
CMSX-4	64.8	9	6	6.5	5.5	6.5	0.1	1	0.6	0	0	0	1312	1382

Table 2	Electrical con	ductivity and	dynamic	viscosity	based on	the related	allovs	CM247-LC and	CMSX-4
I able 2	Electrical con	iductivity and	uvnamic	VISCUSITY	Dascu OII	uic iciaicu	anovs	CM24/-LC and	CM3A-4

Symbol	ymbol Value Dimension	Unit	Source	A low specific electrical resistance is favorable to maximize Ha. The experimentally						
ρ	1.45	10 ⁻⁶	Ωm	[47]	verified values end at ~ 1250 °C being below the solution temperature of the γ' precipitations and the liquidus temperature. The selected value represents the last reading in [47] and is judged as conservative estimate					
σ	6.9	10+5	1/(Ωm)	-	Reciprocal of the specific electrical resistance $(1/\rho)$					
Dynamic	viscosity	from CM247-L	C							
η 6.92	10^{-3}	Pa [52]		A low dynamic viscosity is favorable to maximize Ha. The working point of $1407.5~^{\circ}$ C is selected from the lower measuring limit in [52] and thus near the liquidus temperature in reference to Table 1						

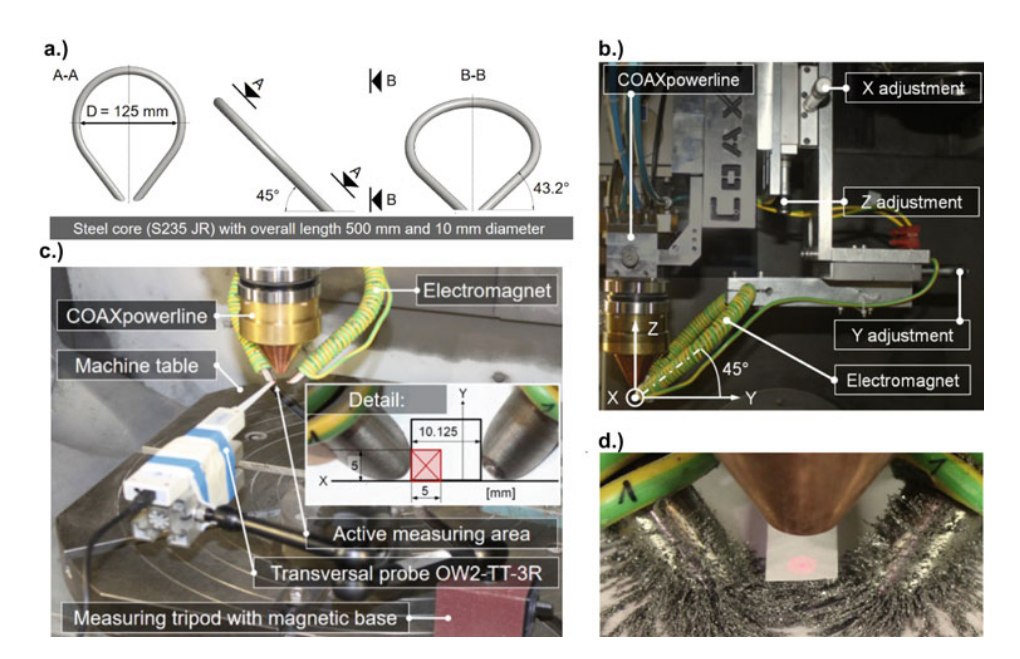


Fig. 4 a Geometry of the S235 JR steel core; **b** electromagnet integrated in the Hermle C 800 U machining center with adjustment units for positioning in relation to the process head of type Fraunhofer IWS COAXpowerline; **c** setup for measuring the magnetic flux density by means of a magnetometer of type KOSHAVA 5 fixed

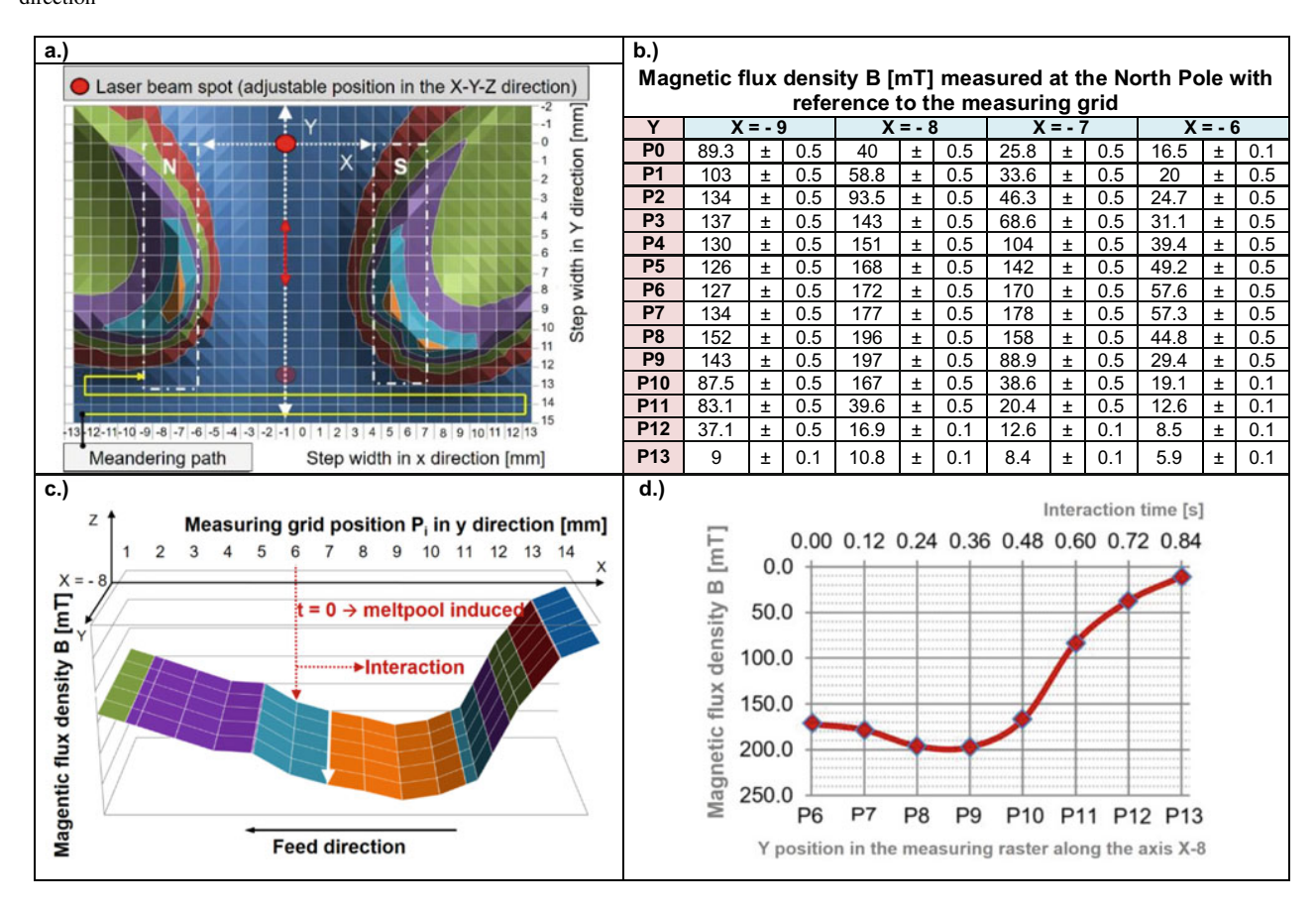
on the machine table with a detail of the pole shoes showing the pole shoe distance in the X direction and the size of the transversal probe OW2-TT-3R measuring tip; \mathbf{d} illustration of the penetration of the laser-induced melt pool by magnetic field lines using the pilot laser (2 red concentric circles) and iron filings for visualization

System Settings and Process Parameters

The magnetic flux density (c.f. Figure 4e) was measured by moving the Z-axis of the machining center step by step in the X or Y direction (Fig. 4b), while the transversal probe (Fig. 4c) remained stationary. The applied step size for meandering the magnetic poles of the electromagnet in the X–Y plane is 1 mm, which corresponds to the measurement grid shown in Table 3a. As a consequence, the values of the magnetic flux density were measured and recorded in each position of the grid. As an example, the magnetic flux density distribution of the north pole of the electromagnet is shown in Table 3b in reference to Table 3a. The red dot at

the intersection of the X and Y axes (Table 3a) symbolizes the laser beam, which is fixed to the Z-axis of the machining center (Fig. 4b, d). The magnetic flux density profile can be positioned in relation to the laser spot by adjusting the inductor along the Y-axis (Fig. 4b). The maximum measured magnetic flux density is 197 ± 0.5 mT and thus about 100 mT below the target estimate (c.f. section "Attempt to Evaluate Effectiveness"). In this study, laser metal deposition is used as a build-up welding process. It is distinguished by the continuous supply of the feedstock material, in this case in the form of powder. A comprehensive characterization of the applied Mar-M-247 powder is provided by Seidel et al. [1]. The powder, however, is transported to the process

Table 3 a Visualization of the magnetic flux density distribution, the meandering path of data acquisition including measuring grid and illustration of the adjustable position of the laser beam spot; **b** measured values and measuring range depending tolerances for the magnetic flux density measured at the magnetic north pole for an excitation current of 60 A supplied by the power source of type Xantrex XFR 20–60; **c** extract of the magnetic flux density from the magnetic north pole with illustration of time t = 0 when the melt pool was induced showing interaction and feed direction; **d** interaction time based on a feed rate of 500 mm min⁻¹ and showing the maximum possible flux density perpendicular to the feed direction.



zone by a carrier gas, in this case argon, using a powder feeder (GTV type PF 2/2). The powder feed rate was selected as 1 g min⁻¹. As the laser beam source, a disk laser with a maximum power of 1 kW is used (Trumpf TruDisk 1000). A 10-m-long fiber optic cable of type LLK-D enables the connection between the power source and the process head. The collimation and focusing is achieved by optical elements with the configuration of $f_{\text{foc}} = 200/f_{\text{coll}} = 200$ (Laserline). The resulting beam diameter in the working plane is adjustable between 1.35 and 1.85 mm, thus being below the target estimate of 2 mm (see section "Attempt to Evaluate Effectiveness"). In fact, a smaller value is rather unfavorable, since the assumed characteristic length (L in Eq. 1) is reduced. On the other hand, the values are determined by the existing optical system. Either way, the feed rate was chosen as 500 mm min⁻¹, applying a laser power of 600 W. As a consequence, two cases were considered in this

investigation. The first configuration uses the smaller beam diameter (~ 1.35 mm), resulting in a shorter characteristic length but at the same time increasing the energy density. However, the temporal change of magnetic flux density for the interaction duration of 0.84 s is shown in Table 3c. The duration and the chosen interval of interaction are based on the characteristic of the electromagnet (Table 3a, b), while both were chosen in relation to the typically prevailing cooling rates in the range of $10^3 - 10^6$ Ks⁻¹.

Results

Individual weld tracks were manufactured by means of laser metal deposition with powder. The track width in configuration 1 (Fig. 5a–f) is about 1 mm independent of the magnetic field influence. The track width in configuration 2,

also being independent of the magnetic field influence, is in the range of 1.9 mm (Fig. 5g-l). The selected weld bead width-to-depth ratios are significantly greater than the recommendations in the literature (ratio recommendation $\gg 1$). In summary, the selected melt pool dimensions are based on experience in the field of tip repair at turbine blades. Nevertheless, the single beads welded without influence of the magnetic field without exception show pronounced crack structures in the center (Fig. 5a-c). Observation of the crack flanks provided a good match of the opposite contours with isolated protruding tips indicating local bridging. The tips, however, show no fractured surfaces which may be attributed to a subsequent rounding from remaining interdendritic melt. Furthermore, the samples show liquation cracks emerging from the partially melted zone (PMZ). The weld beads shown in Fig. 5d-f, on the other hand, solidified under the influence of the magnetic field described in section "System Settings and Process Parameters." These weld beads show no such distinct hot crack formation in the center of the welds. Nevertheless, the samples with magnetically influenced solidification show liquation cracks emerging from the PMZ similar to the uninfluenced samples. This does not seem to be a contradiction since the probability of a lack of melt supply is rated higher in the PMZ than in the actual melt pool. However, in order to avoid liquation cracking in a second series of experiments, the substrate surface was remolded into a thin layer to achieve chemical homogenization prior the deposition of weld beads. This is in reference to the effect of planar solidification resulting from a positive thermal gradient and a heat flow pointing from the inside of the melt pool of the melt pool toward the lower-temperature substrate below [1]. Either way, single weld beads were deposited on the previously remelted surfaces, while the beam diameter in the working plane was increased to 1.85 mm (configuration 2) in reference to the estimate of 2 mm formulated in section "Attempt to Evaluate Effectiveness." Figure 5g-i show the results of the magnetically unaffected weld beads, again showing distinct hot cracking. Liquation cracking, however, could not be avoided, which is inter alia attributed to an insufficient thickness of the remolded layer with respect to the weld penetration depth. The comparative welds deposited under the influence of the magnetic field (Fig. 5k-n), on the other hand, show no formation of hot cracks, but isolated liquation cracks, which correlates with the first series of experiments. Analogous to the samples welded without magnetic influence, this aspect is linked to the insufficient thickness of the remolded layer. Striking, however, were the clear differences in the orientation of the primary dendritic arms exemplified in representative details shown in Fig. 5m, n.

Fig. 5 Light microscopy images from cross sections of Mar-M-247 ▶ single weld beads on the same substrate achieved by LMD with powder a-c without the influence of an external magnetic field; d-f with the influence of an external magnetic field according to section II.II; g-i without the influence of an external magnetic field but with previous melting of the substrate surface; j-I with the influence of an external magnetic field and previous melting of the substrate surface; m typical orientation of the primary dendrites without magnetic field influence; n typical orientation of the primary dendrites with magnetic field influence

Conclusion

- Experimental determination of the thermophysical constants in the temperature range of the laser-induced melt pools is required for a well-founded assessment of effectiveness and/or accompanying simulation,
- No contradictions were identified with regard to the line of argument that led to the selected method using the specially developed system technology,
- Hot cracking is drastically reduced under the influence of the magnetic field while liquation cracking occurs for all approaches,
- The values for the melt pool width and the magnetic flux density, which were determined in the attempt to evaluate effectiveness section, were noticeably undercut but promising results have been achieved,
- Nevertheless, in accordance with the line of argument the presented approach led to a reduction in hot cracking whereas the clarification of the underlying causes requires further research,
- Based on the available results it is recommended to increase the width of the melt pool while the thickness should be maintained or reduced, while, at the same time, the magnetic flux density should be increased,
- In addition, the laser beam power and intensity distribution should be designed in such a way, that the Marangoni convection is reinforced,
- Moreover, the depth of the chemical homogenization by adequate remolding, performed prior the deposition of a weld bead, should be matched to the weld bead penetration depth in order to potentially avoid liquation cracking.

Outlook

On the basis of the results achieved, a test stand is realized which enables a magnetic flux density of 1 T in an air gap of 10 mm. The achievable field homogeneity is \pm 5% within a

